A Comprehensive Approach to Design of the NF106B-VST Model Follower System

HAROLD H. BURKE*
Army Materiel Systems Analysis Agency, Aberdeen Proving Ground, Md.

AND

ORRIN C. KASTE†
Ballistic Research Laboratories, Aberdeen Proving Ground, Md.

AND

BARTLETT WONG‡
Transportation System Center, Cambridge, Mass.

A summary of the procedures used to design the high-performance model follower flight control system of the NF106B-VST is presented. Major phases included design criteria/performance index development, rigid/elastic mathematical model development, initial design analysis and simulation, hardware design and implementation, final design verification simulation, flight hardware installation, and flight test evaluation. The design/synthesis procedure used root-locus methods for selecting gains and compensations, frequency response methods for determining gain and phase margins, and analog simulation for verifying transient response. Actual hardware characteristics were measured and incorporated into the final design verification simulation. Through planned iterations it was possible to apply complementary analytical techniques effectively and factor updated information into the problem, thereby producing a successful design in a relatively short time span. Flight test data are presented to illustrate results obtained.

I. Introduction

THE Martin Marietta Corporation recently completed modification and flight testing of two F-106B delta wing aircraft for use as aerospace vehicle trainers at the Aerospace Research Pilot School at Edwards Air Force Base, Calif. The trainers are known as NF106B-VST (variable stability trainers). Their primary purpose is to provide realistic in-flight simulation of a variety of existing or proposed vehicles. The modification contract specified that the model follower approach be used to obtain variable stability capability and also specified the model state variables that were to be used.

The primary purpose of this paper is to describe a comprehensive approach to design used to synthesize the model follower loops employing conventional techniques in a planned coordinated effort. This approach resulted in a successful practical design in a relatively short time span, and avoided problems commonly encountered in control system work, e.g., performance deficiencies; inadequate understanding of system characteristics; and instability, particularly involving structural modes. The intent of this paper is to illustrate and emphasize the importance and need for considering all facets of a control design problem, including the effects of knowledge obtained as the design and testing phases progress. It is not intended to discuss or defend the use of particular follower loops in the NF106B-VST or to emphasize VST performance characteristics.

Presented as Paper 69-886 at the AIAA Guidance, Control and Flight Mechanics Conference, Princeton, N.J., August 18-20, 1969; submitted August 27, 1969; revision received April 13, 1970. This work was performed as a part of USAF Contract AF41(608)-38704 NF106B-VST program when the authors were employed by the Martin Marietta Corporation, Baltimore, Md.

* Senior Professional Staff Member.
† Chief, Information and Control Theory Branch.
‡ System Simulation Group. Member AIAA.

The design objective of this effort was to develop a model follower flight control system capable of following the model state variables: i.e., lateral acceleration-A_Y (cruise and landing system); roll angle-ϕ (cruise and landing system); normal acceleration-A_Z (cruise system); altitude and short period pitch angle-$h + \theta_{sp}$ (landing system).

II. Comprehensive Approach to Design

Major Phases

The design approach used is illustrated in Fig. 1. The major phases of work are outlined as follows:

1) Design Criteria/Performance Index Development: Considerations include system stability, steady-state and transient performance, saturation, and cross-talk effects.

2) Mathematical Model Development: Includes rigid plus elastic body and a general control law including major system nonlinearities.

3) Initial Design Analysis and Simulation: A process of repetitive analysis where a combination of root locus, frequency response, and analog simulation techniques are exercised iteratively by the design engineer.

4) Hardware Design and Implementation: This phase, which is very important to the overall design effort, is not covered in this paper.

5) Final Design Verification Simulation: This phase is an analog simulation which includes the actual hardware characteristics which finally evolve from the hardware design effort.

6) Flight Hardware Installation: Includes hardware changes resulting from the previous phase.

7) Ground and Flight Test Evaluation: This phase verifies predicted behavior and/or indicates design modifications.

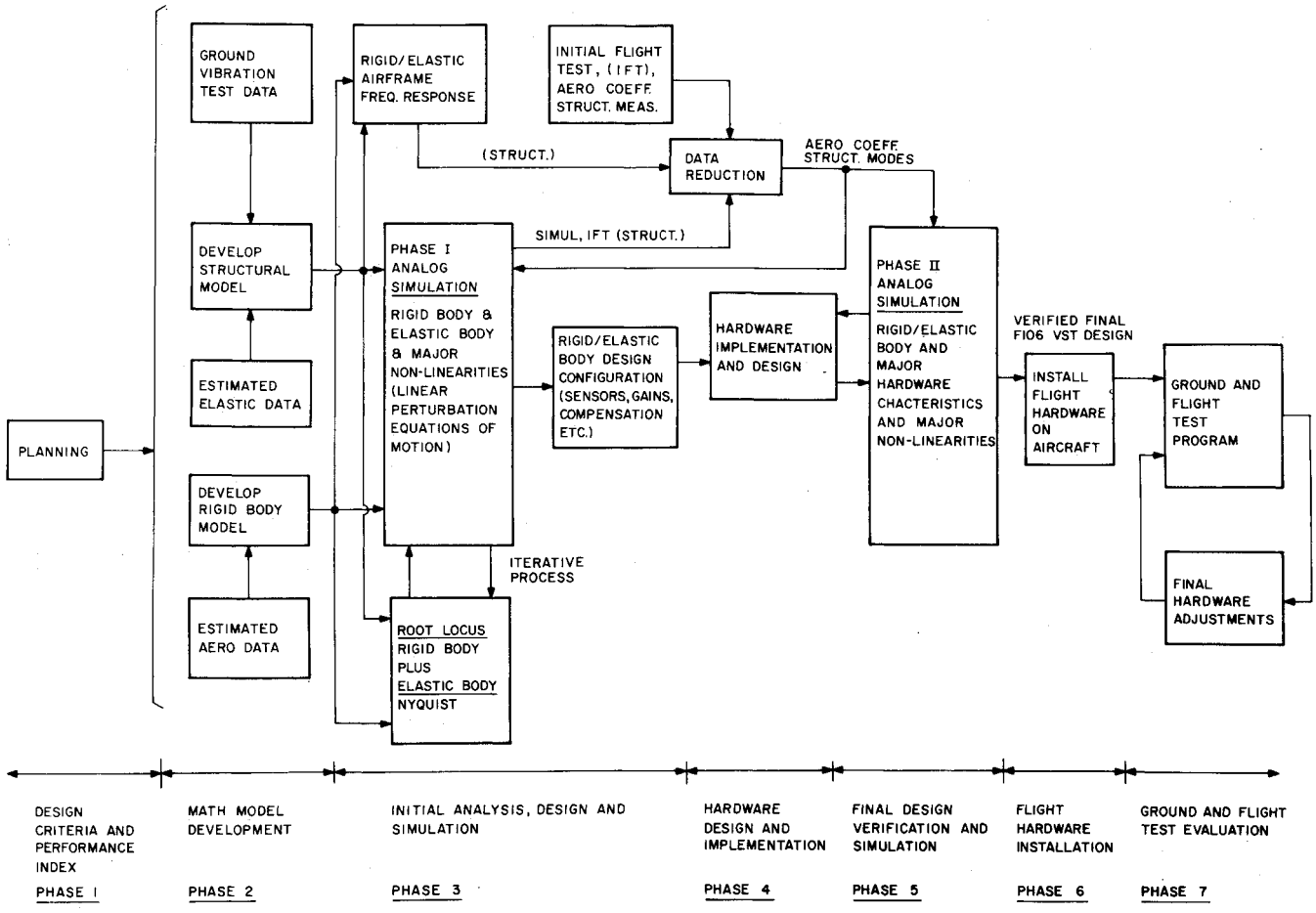

Fig. 1 Major phases of comprehensive approach to design.

Rationale of Design Approach

The design criteria must guarantee asymptotic stability of all modes, and then assure the "best" transient response, with a minimum of cross-talk. The design criteria/performance index, mathematical model, and design/synthesis techniques employed cannot be chosen independently. The combination must provide the design engineer with good insight to the problem of stability and response. Any assumptions made in the development of the design criteria/performance index and mathematical model must be validated on an a priori basis if possible and must certainly be verified at specific check points during the design process before progressing to the next major phase of work.

With the foregoing rationale in mind, the design/synthesis procedure is based on root locus studies to gain insight for proper feedback gains and compensations, frequency response analyses to determine the actual gain and phase stability margins of the system, and analog simulation studies to verify the adequacy of the design from the standpoint of transient response. This procedure requires a number of iterations with and without nonlinearities before a design can be established. After the initial design has been achieved the hardware is designed and implemented. The actual hardware characteristics are then measured and incorporated into a final design verification simulation. Finally, flight hardware is installed on the aircraft and ground and flight test evaluations are performed.

III. Design Procedure

This section outlines the comprehensive approach to design, emphasizing the procedure rather than the details. The first phase was to establish the basic design criteria/performance index. Consideration of the system performance information most readily observable from conventional analytical techniques led to selection of damping ratio criteria ($\zeta > 0.3$ for $0.1 < \omega < 10$ rad/sec, $\zeta > 0.1$ for all other frequencies, as observed on root locus plots), and phase and gain margin criteria (phase margin $> 30°$ and gain margin > 6 db as observed on Nyquist and Nichol plots). In addition, the design goal was to provide dynamic response which presented no noticeable lag to the pilot, and which was of the correct transient and steady-state magnitude.

In phase 2 the mathematical model of the complete system was formulated. Details are too voluminous for inclusion here; a full description is available in a Martin Company report.[1] The rigid body airframe was represented by the conventional uncoupled longitudinal and lateral/directional equations of motion. The aircraft elastic structural modes were represented by generalized differential equations. Elastic structural data were based on results of ground vibration tests. Five symmetric modes ranging in frequency from 8.3 to 25.3 cps and five antisymmetric modes from 10.5 to 27.0 cps were identified and included in the mathematical model.

The control surface actuator representations were based on ground test data. Sensor characteristics were represented by best data available at initiation of the initial design phase, and were revised prior to the final design verification phase.

The form of the follower loops evolved from a general control law which included all possible linear terms. The unnecessary terms were eliminated during analyses when it was demonstrated that they did not improve the system significantly.

A complete description of the phase 3 effort involving initial design and simulation of the follower loops is too

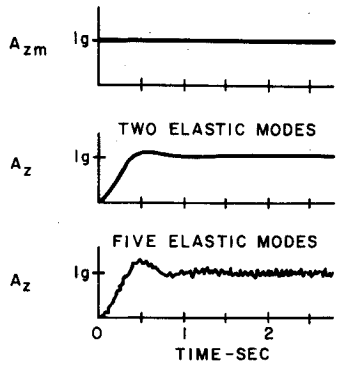

Fig. 2 Response of preliminary A_Z follower loop—cruise flight condition.

extensive for presentation in this paper, but is given in Ref. 1. As a typical example the longitudinal cruise system will be used to illustrate the comprehensive approach to design. Since it would be impractical to include all the analytical data in this paper only selected highlights are used to develop the flavor of the design evolution.

The point of departure for this engineering analysis was the preliminary design work conducted by Systems Technology Inc.[2] A number of major design problems existed because of the nature of the system specified in the contract. For example, an acceleration model following system is inherently sensitive to elastic structural oscillations, especially for the F-106B with its many closely spaced modes. Analyses indicated that all modes were significantly in the design because they were strongly coupled to each other.

Figure 2 shows analog computer traces of the step response of the preliminary A_Z follower loop that was based on rigid body design analysis, when the first two elastic modes and then when five elastic modes were included in the simulation. Note the 160 rad/sec limit cycle due to 5th mode instability. The corresponding root loci of Figs. 3 and 4 show the nature of the problem. The rigid body roots are unaffected by the inclusion of the elastic modes; however, the elastic modes are heavily influenced by higher order system dynamics and by other elastic modes. Figure 3, with only modes 1 and 2 included, and with sensor dynamics neglected, predicted stable elastic modes for $K_{AZ} = 0.0015$ rad/fps^2. Figure 4 shows that the 2nd and 5th modes are unstable when modes

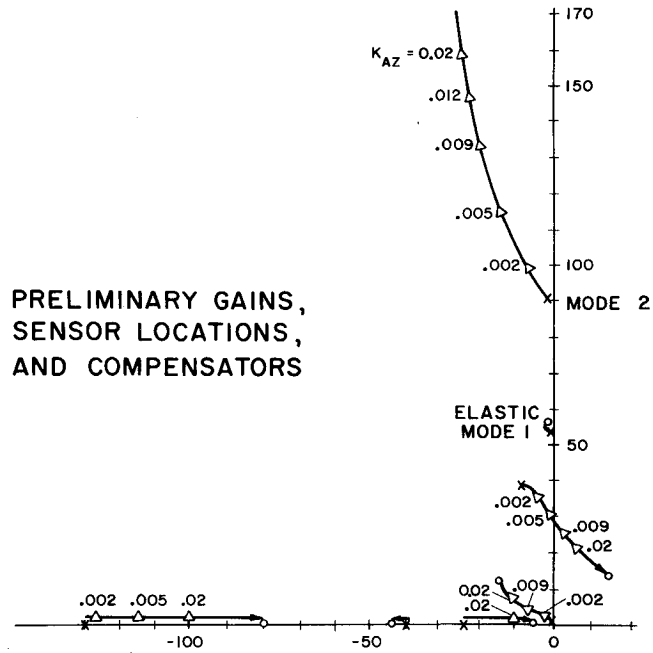

Fig. 3 Root loci for preliminary A_Z follower loop with two elastic modes.

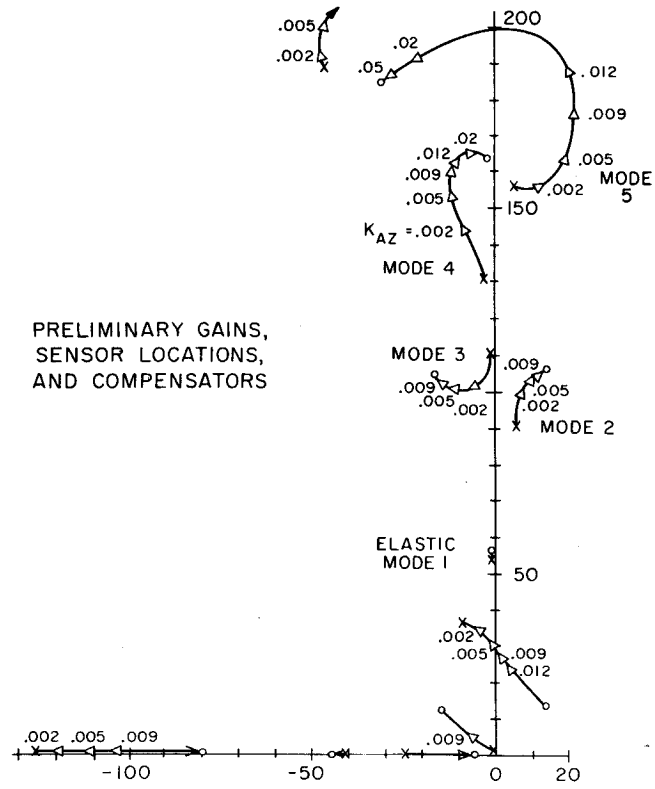

Fig. 4 Root loci for preliminary A_Z follower loop with five elastic modes.

1–5 are included. Evidence of the 2nd mode can be observed as a modulation on top of the 5th mode in the acceleration traces of Fig. 2.

Obviously, gains based on a rigid body model would not be suitable for the elastic representation. To stabilize the

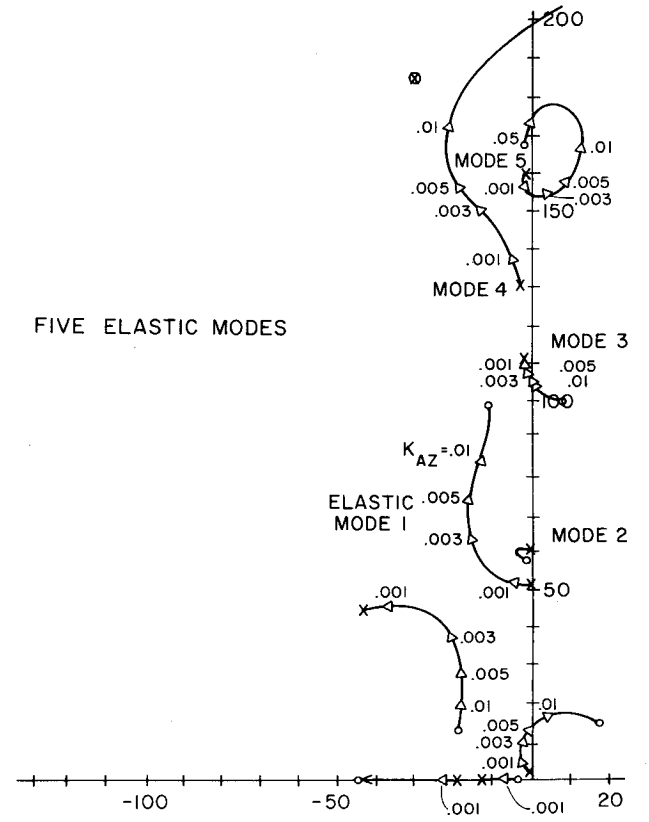

Fig. 5 Root loci for initial A_Z follower loop design without structural filter.

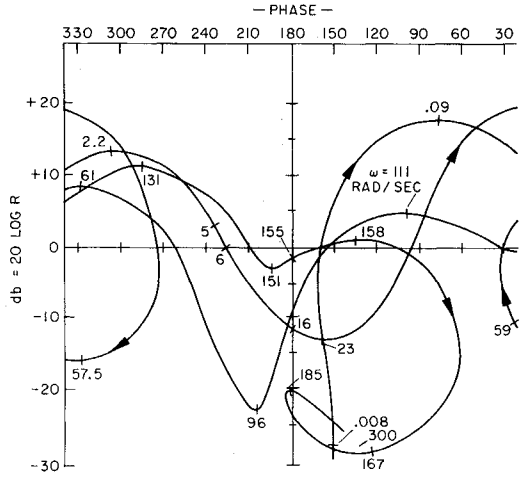

Fig. 6 Nichol's plot for initial A_Z follower loop design without structural filter.

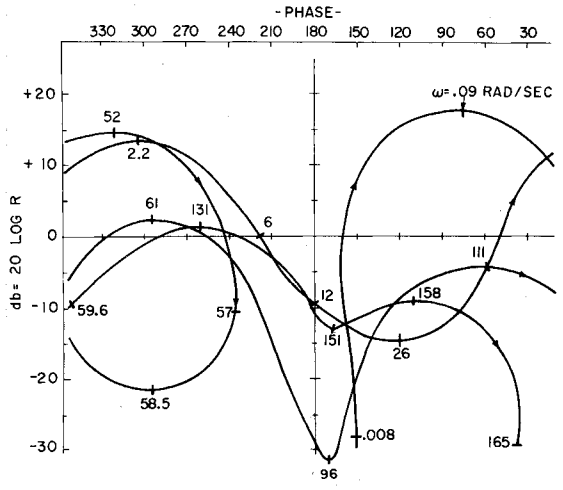

Fig. 8 Nichol's plot for final A_Z follower loop design with structural filter.

structural modes one could change gains and compensators, add filters, or change sensor locations. All three approaches were necessary to achieve a stable system. The evolution can be illustrated in Fig. 5 which shows the root loci for the best sensor locations, and changes in gains and compensators. Note that with these inner loop changes the root locus pattern is changed completely relative to that of Fig. 4 where the branch associated with the actuator pole established the system bandwidth of 30 to 40 rad/sec. For the revised system the bandwidth is controlled by the branch stemming from the F-106B short period pole and is considerably smaller, less than 15 rad/sec. The reduction in bandwidth is necessary to achieve elastic stability. The Nichol's chart for this system with the loop open at the actuator instead of at the acceleration error point, Fig. 6 shows that there is insufficient gain margin.

The next major change was the addition of a structural filter. The root loci for this system are shown in Fig. 7 and the Nichol's plot is shown in Fig. 8. Here the minimum stability margins are 40° in phase and 10 db in gain.

After a number of iterations of the root locus/analog simulation/frequency response process, including an extensive parametric sensitivity study, necessitated by the large number of parameter combinations involved and the subsequent availability of an updated data package, the initial design configuration was used to design and implement the hardware of the model follower system (phase 4). The hardware characteristics were then measured for inclusion in the final design verification simulation.

The final design verification, phase 5 of the procedure, consisted of an analog simulation using updated values of system parameters. This study was planned as part of the design effort because it was anticipated that the follower loop hardware would not exactly match the design values; that updated data would be available on airframe, aerodynamic, structural, and mass characteristics; and that verification of possible design improvements would be required. The updated system parameters did not require significant changes to the design of the A_Z follower loop. Final design parameters were incorporated in the hardware, and the flight system was installed in the aircraft as phase 6 of the effort.

Phase 7, the ground and flight test program, was an essential part of the design verification process. Initial tests were largely devoted to checking stability of the system and observing basic operating characteristics. Some difficulty

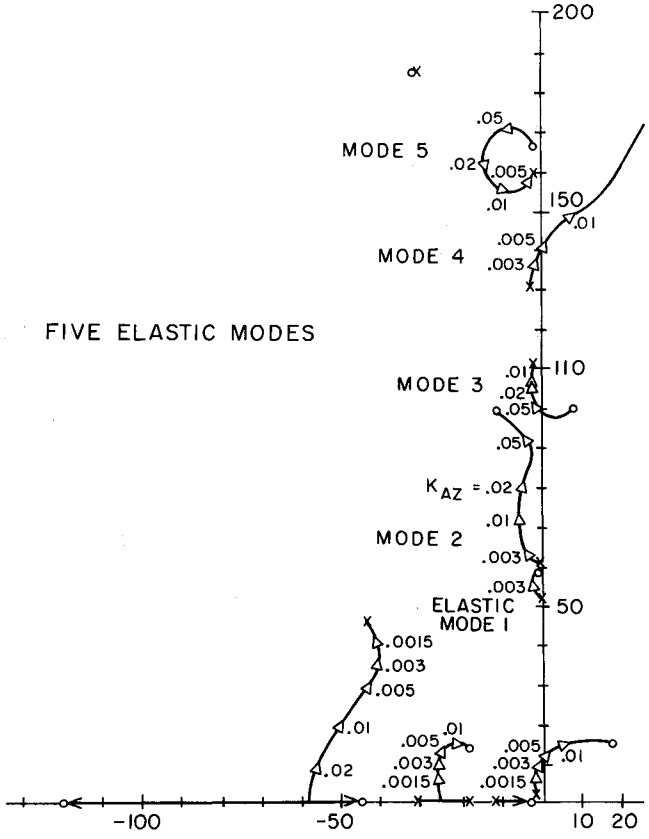

Fig. 7 Root loci for final A_Z follower loop design with structural filter.

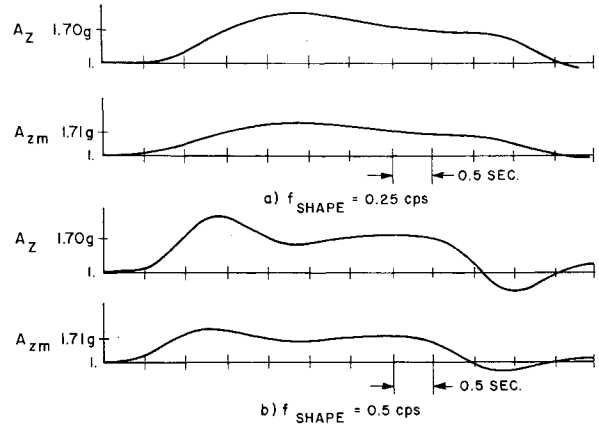

Fig. 9 Response of A_Z follower loop, flight system, cruise flight condition, 350 knots at 20,000 ft.

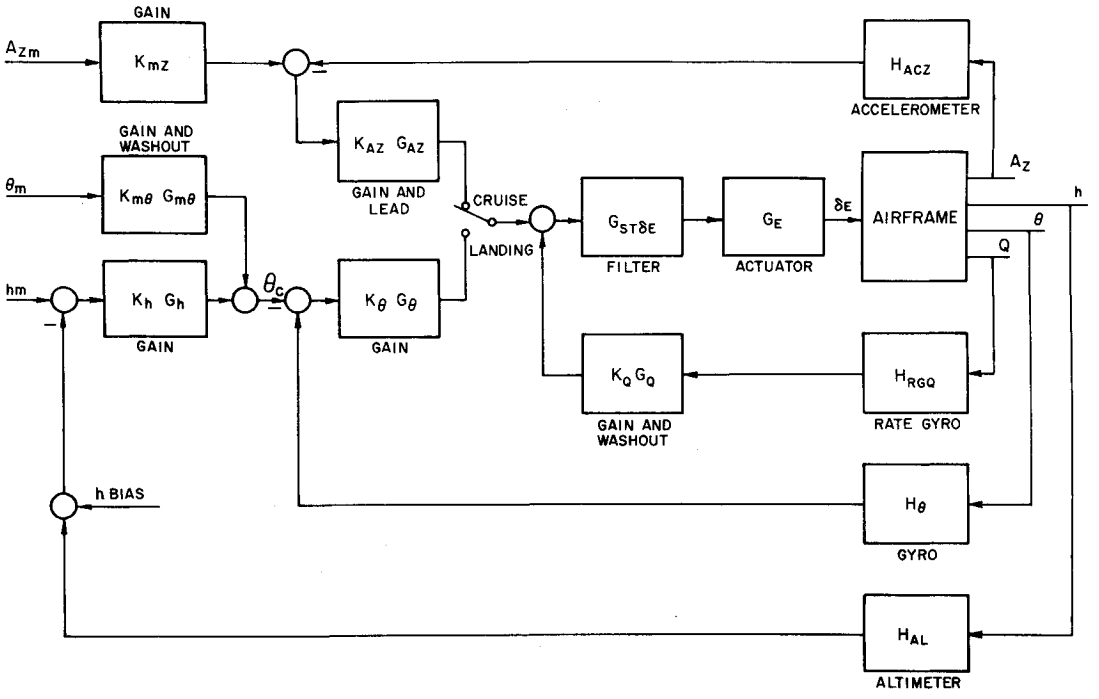

Fig. 10 A_Z **and** h **follower loops.**

was encountered with elastic mode oscillations during early ground and flight tests. These oscillations were due to structural modes at frequencies above those of the ten modes identified and included in the mathematical model used in the design process. The problem was overcome by making gain and filter modifications to the final system.

A series of flight tests was conducted using inputs to the follower loops which were the same as those used in the analog simulation studies. This procedure was chosen to permit direct comparison of flight system performance with that obtained in the analog design studies. Figure 9 shows responses of the flight A_Z follower loop to shaped commands of two different frequencies. Response is good, with only a slight lag evident. Ultimate flight verification of follower loop performance was obtained by simulating F-106B and X-24A lifting body characteristics in the model computer and observing responses of the NF106B-VST. Simulation of the F-106B permitted a direct check on over-all simulation fidelity, and simulation of the X-24A permitted a check on the capability of the system to simulate a vehicle that is quite different from the F-106B. Evaluation of flight test results was obtained qualitatively from test pilot observations, and quantitatively from recorded instrumentation signals.

IV. Design Summary

The comprehensive approach to design just described for the A_Z follower loop is essentially an organized iterative process that produces a system satisfying the design criteria/performance index. This approach was also used to design the h, A_Y, and ϕ follower loops. Details of the method will not be presented here, but success of the approach will be illustrated by presenting a summary of the over-all configuration and its performance.

Table 1 A_Z **and** h **follower loop parameters**

Symbol	Final system	Flight system
K_{mZ}	1.25	1.40
$K_{m\theta}$	1.0	1.5
$G_{m\theta}$	$2s/(1+2s)$	$2s/(1+2s)$
K_h	0.0006 rad θ_c/ft	0.006
G_h	1	1
K_{AZ}	0.0015 rad/ft/sec^2	0.0014
G_{AZ}	$(1+0.33s)/(1+0.08s)$	$(1+0.33s)/(1+0.125s)$
K_θ	0.8	0.8
G_θ	1	1
$G_{ST\delta E}$	$(1+s/125)/(1+s/30)$	$(1+s/200)/(1+s/30)$
K_Q	0.075 cruise 0.24 landing	0.072 0.23
G_Q	$2s/(1+2s)$	$2s/(1+2s)$

The basic block diagram of the normal acceleration and altitude follower loops is shown in Fig. 10. The normal acceleration of the model (A_{Zm}) forms the input to the system in the cruise mode, and the model altitude (h_m) and pitch angle (θ_m) form inputs to the system in the landing mode. The pitch signal passes through a washout filter so that only short pitch signals are fed to the follower loop. Parameter values for these loops are given in Table 1.

For comparison, values are given as determined after the final design verification (phase 5) and as established after completion of flight tests (phase 7). The change in K_{mZ} was made to bring the A_Z response to the proper level, and the change in $K_{m\theta}$ was dictated by pilot preference. Changes in G_{AZ} and $G_{ST\delta E}$ were made to prevent high-frequency elastic mode oscillations which occurred during ground tests of the system.

Performance of the h follower loop is illustrated in Fig. 11 for the final design and flight systems. The steady-state error is inherent in the system for ascending or descending flight. The jerkiness evident in the flight data arises from altitude sensor resolution characteristics.

The block diagram of the lateral acceleration and roll

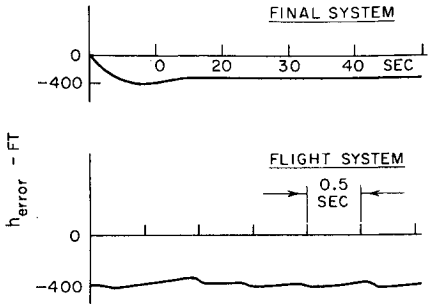

Fig. 11 Response of h **follower loop, flight system, 6000 fpm descent.**

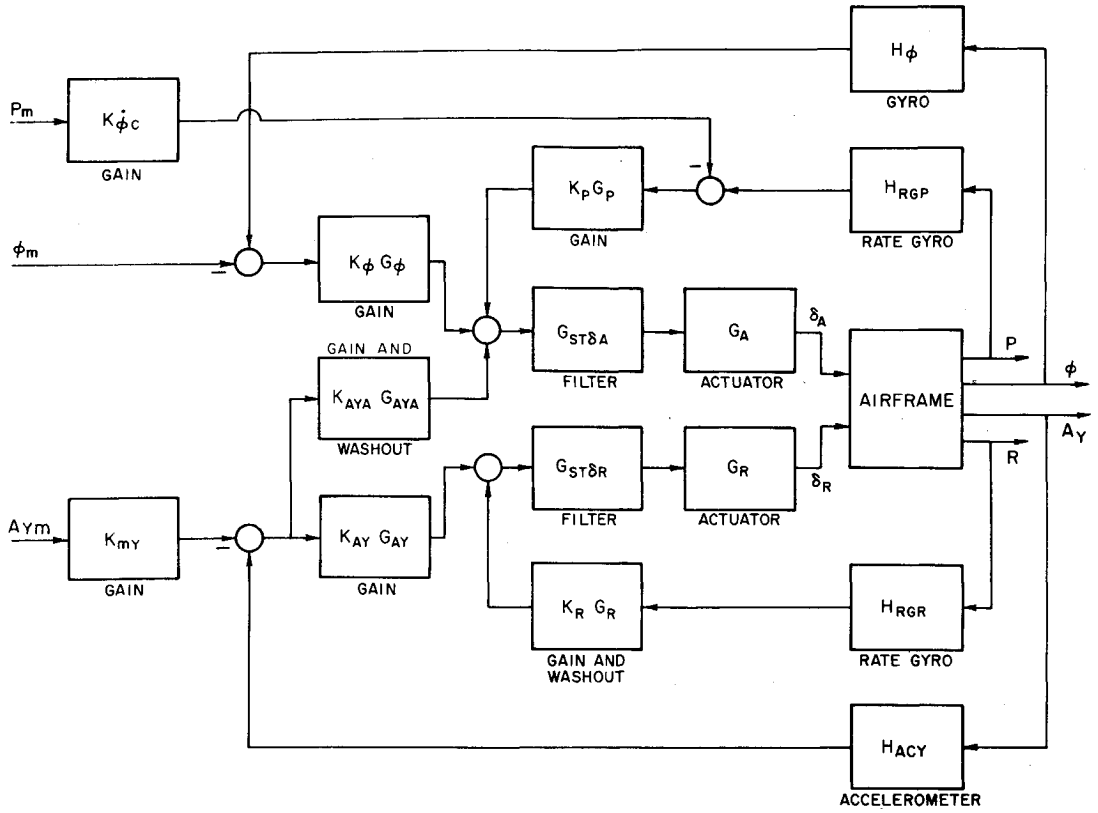

Fig. 12 A_Y and ϕ follower loops.

angle follower loops is shown in Fig. 12. The lateral acceleration of the model (A_{Ym}) forms the input to the A_Y loop, and the roll angle of the model (ϕ_m) forms the primary input to the ϕ loop. Parameter values for these loops are given in Table 2.

The values listed for the system as defined after the final design verification (phase 5) reflect changes made relative to the initial design. These changes included addition of a roll rate feedforward ($K\dot{\phi}_c$) to improve response of the ϕ loop, reduction of K_{AY} and changes in $G_{ST\delta R}$ to eliminate a 44 cps limit cycle oscillation previously evident in the A_Y loop and change of G_R and relocation of the aileron crossfeed path to improve response of the A_Y loop. Additional changes in the flight system were largely the result of difficulties with structural oscillations at frequencies above those considered in the design analyses. Changes were required in the rudder structural filter $G_{ST\delta A}$ along with a reduction in K_{AY} in order to prevent oscillations involving the lateral accelerometer. This was accomplished without significantly affecting A_Y response, although K_{mY} had to be increased to achieve the correct level.

An illustration of the performance achieved by the flight A_Z, A_Y and ϕ systems operating simultaneously is presented in Fig. 13, where responses are shown for a case when the pilot maneuvered the model into a wind-up turn. Over 500 "runs" were made by experienced pilots during test and demonstration flights. Pilot comments on follower loop performance were very favorable.

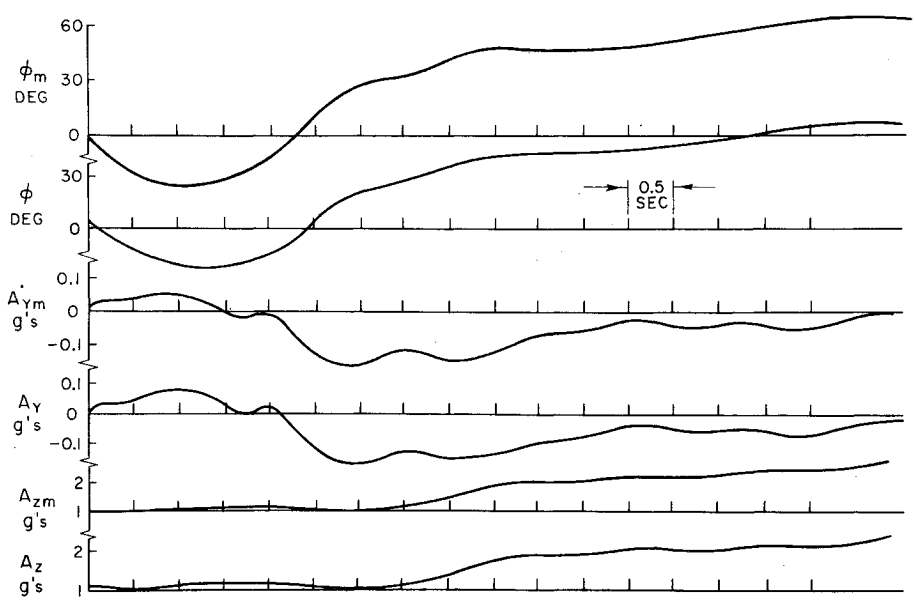

Fig. 13 Simultaneous response of ϕ, A_Y, and A_Z follower loops, flight system, 350 knots at 20,000 ft.

Table 2 A_Y and ϕ follower loop parameters

Symbol	Final system	Flight system
$K_{\dot{\phi}c}$	0.5	0.7
K_{mY}	1.2	1.67
K_ϕ	0.8	0.77
G_ϕ	1	1
K_{AYA}	0.004 rad/fps^2	0.0038
G_{AYA}	$5s/(1+5s)$	$5s/(1+5s)$
K_{AY}	0.07 rad/fp^2	0.04
G_{AY}	1	1
K_P	0.2	0.17
G_P	1	1
$G_{ST\delta A}$	$(1+s/250)/(1+s/62.5)$	$(1+s/300)/(1+s/30)$
$G_{ST\delta R}$	$(1+s/400)/(1+s/250)$	$(1+s/300)/(1+s/125)$
K_R	1	0.8
G_R	$2s/(1+2s)$	$2s/(1+2s)$

V. Summary

The NF106B-VST modification and flight program provided an excellent opportunity to demonstrate the success of a comprehensive approach to design of a high performance flight control system. By using a planned iterative procedure it was possible to apply several complementary analytical techniques effectively, and to factor updated information into the problem readily. Emphasis was placed on developing a complete yet workable mathematical model including high frequency dynamics where data were available. This proved valuable in diagnosing and solving problems which arose during simulation and testing phases of the program. Pilot opinions and recorded flight test data indicated that the system resulting from the effort described in this paper performs very well.

References

[1] Wong, B., Burke, H., Hutton, M., and Farris, R., "NF106B-VST Model Follower and Structural Protection System Design," ER 14278, Feb. 1967, Martin Marietta Corp., Baltimore, Md.

[2] Teper, G. L. and Jex, H. R., "Feasibility of Using F-106B Aircraft for a Variable Stability Trainer," STI 136-1, March 1965, Systems Technology Inc., Hawthorne, Calif.

JUNE 1971 J. AIRCRAFT VOL. 8, NO. 6

Hover and Forward Speed Aerodynamics of Several Tracked Air-Cushion Vehicle Models

HENRY W. WOOLARD,* KWAN L. SO,* AND RICHARD J. SERGEANT†
TRW Systems Group, Redondo Beach, Calif.

Hover and moving-ground-plane wind-tunnel tests were performed on three elongated Tracked Air-Cushion Vehicle (TACV) models and one circular air-cushion model in a joint TRW-NASA Langley test program. Selected results are presented for all the models tested in hover and for one of the elongated models tested at forward speed. Separate force and moment measurements on the body and cushions were taken. The air-cushion lifting performance in hover was found to be influenced by cushion length-to-width ratio, cushion-jet Reynolds number, and body-shell proximity. At a fixed cushion height and constant air-flow rate, cushion lift generally increased with forward speed to a peak value and then decreased. This characteristic diminished with increasing cushion height. For the elongated model at forward speed, the body forces, and moments generally were greater than those of the cushion except for the lift and pitching moment.

Nomenclature

A_c = air-cushion base area
C_L = body lift coefficient, $L_b/q_\infty S_m$
C_m = body pitching-moment coefficient, $m_b/q_\infty S_m l_b$
C_p = pressure coefficient, $(p-p_\infty)/q_\infty$
d_m = diameter of a circle having an area equal to the body maximum cross-sectional area
h = air-cushion edge height
h^* = height parameter, $h/t(1+\sin\gamma)$ or $1/t^*$
H = total pressure (absolute)
$\bar{k}_B'$ = belt forward-speed parameter, $q_B/(\bar{p}_c-p_\infty)_o'$
$\bar{k}_F, \bar{k}_F'$ = air-cushion forward-speed parameter, $q_\infty/(\bar{p}_c-p_\infty)_o, \bar{q}_\infty/(\bar{p}_c-p_\infty)_o'$
$\bar{K}_c'$ = air-cushion mean-pressure parameter, $(\bar{p}_c-p_\infty)_o'/(H_p-p_\infty)$
K_Q = normalized air-flow rate [see Eq. (1)]
l = length
l = rolling moment about the x axis; positive, using a left-hand rule
L = lift force (see text)
L_k = air-cushion lift due to body cavity pressure, $(\bar{p}_c-\bar{p}_k)A_c$
L_M = lift measured by strain-gauge balance
$(L_c)_0$ = cushion lift in hovering state
m = pitching moment about an axis parallel to the y axis; positive, using a right-hand rule (see Fig. 1 for moment centers)
n = yawing moment about an axis parallel to the z axis; positive, using a left-hand rule (see Fig. 1 for moment centers)
p = static pressure (absolute)
$(\bar{p}_c-p_\infty)$ = air-cushion mean gauge pressure

Presented as Paper 69-750 at the CASI/AIAA Subsonic Aero- and Hydro-Dynamics Meeting, Ottawa, Canada, July 2–3, 1969; submitted July 11, 1969; revision received February 25, 1970. This work was supported by the Office of High Speed Ground Transportation, U.S. Department of Transportation, under Contract C-353-66(NEG). The technical contributions of K. J. Grunwald, D. Hammond, and R. E. Kuhn, participants for NASA, are gratefully acknowledged.

* Member of Technical Staff, Aerothermodynamics Department, Aerosciences Laboratory. Members AIAA.

† Member of Technical Staff, Aerothermodynamics Department, Aerosciences Laboratory.